Pure Appl. Geophys. 172 (2015), 309–331

DOI 10.1007/s00024-014-0901-0

Pure and Applied Geophysics

Crustal Thickness of Iran Inferred from Converted Waves

Fataneh Taghizadeh-Farahmand,[1] Narges Afsari,[2] and Forough Sodoudi[3]

Abstract—The Iranian plate is part of the Alpine-Himalayan orogenic belt, which has been formed by the continental collision between the Arabian and Eurasian plates. The present-day Iranian plate is characterized by diverse tectonic domains including mountain belts (e.g. Zagros and Alborz, Kopeh-Dagh) and oceanic plate subduction (e.g. Makran). Here we present the lateral variations of the Moho discontinuity beneath Iran using a detailed P receiver function study. Our results allow for more precise estimations of the crustal thickness and enable us to provide a detailed Moho depth map for all of Iran for the first time. We used the teleseismic events recorded from 1995 to 2011 at 77 national permanent stations (24 broadband and 53 short period stations). Our results show significant variations in the crustal thickness, which are related to the different geological features within Iran. In general, the average crustal thickness beneath Iran is about 40–45 km. A relatively thick crust of about 54 $\pm$ 2 km due to the shortening is observed beneath the Alborz mountain ranges. The crust beneath the Alborz zone shows a thickness changing from 47 $\pm$ 2 to 45 $\pm$ 2 km from west to east and reaches a thickness of about 50 $\pm$ 2 km beneath the Kopeh-Dagh mountain range. We find the thinnest crust of about 33 $\pm$ 2 km beneath the Makran subduction zone in southeast Iran showing a normal continental crust, which has not been influenced by collisional processes. The thickest crust ($\sim$66 $\pm$ 2 km) is locally observed beneath the Sanandaj-Sirjan Zone, which is considered the suture zone of the collision between the Arabian and Eurasian plates.

Key words: Iran, Moho depth, P receiver function, modeling.

Abbreviations

MZTF	Main Zagros Thrust Fault
SSZ	Sanandaj-Sirjan Zone
ZFTB	Zagros Fold and Thrust Belt
UDMA	Urumieh-Dokhtar Magmatic Arc
CIMC	Central Iranian Micro-Continent

[1] Department of Physics, Qom Branch, Islamic Azad University, Qom, Iran. E-mail: f_farahmand@qom-iau.ac.ir
[2] Department of Engineering Faculty of Civil Engineering Nowshahr Branch, Islamic Azad University, Mazandaran, Iran.
[3] Helmholtz Centre Potsdam, GFZ German Research Centre for Geosciences, Telegrafenberg 14473, Potsdam, Germany.

1. Introduction

The continental collision between the Arabian and Eurasian plates results in a complex deformation within Iran, which is controlled by the continuing convergence of the Arabian plate toward the Eurasian plate. The present-day Iranian plate indicates different tectonic processes including orogeny (Zagros, Alborz, and Kopeh-Dagh) and subduction of the oceanic lithosphere (Makran) (Fig. 1). The collision between the Arabian and Eurasian plates started in the early Miocene, after the Neotethys Ocean was subducted beneath Eurasia (Jackson and McKenzie, 1984; Dewey *et al*., 1986; Beghoul and Barazangi, 1989; Boulin, 1991). The closure of the Neotethys Ocean resulted in the emplacement of ophiolites along the Zagros suture zone and the onset of deformation in the Zagros fold and thrust belt (Stoneley, 1981; Richards *et al*., 2006). The collision process trapped the central Iranian block between the Arabian plate in the south and the Turan shield in the north and led to intra-continental shortening, formation of the Iranian plateau, widespread deformation, and mountain building (Bird, 1978). It is assumed that most deformation is accommodated not only in the major mountain belts (Zagros and Alborz) with large reverse faults, but also along large strike-slip faults that surround the blocks (the Central Iranian block, the Lut block, and the southern Caspian Sea, see Fig. 1) (Jackson and McKenzie 1984; Berberian and Yeats 1999). Distribution of seismicity and the local topography occur at the edges of the deformation zones, which are well defined by previous studies (e.g. Jackson and McKenzie, 1984).

The depth of Moho is an important parameter to characterize the structure of the crust. Furthermore, it provides significant constraints on

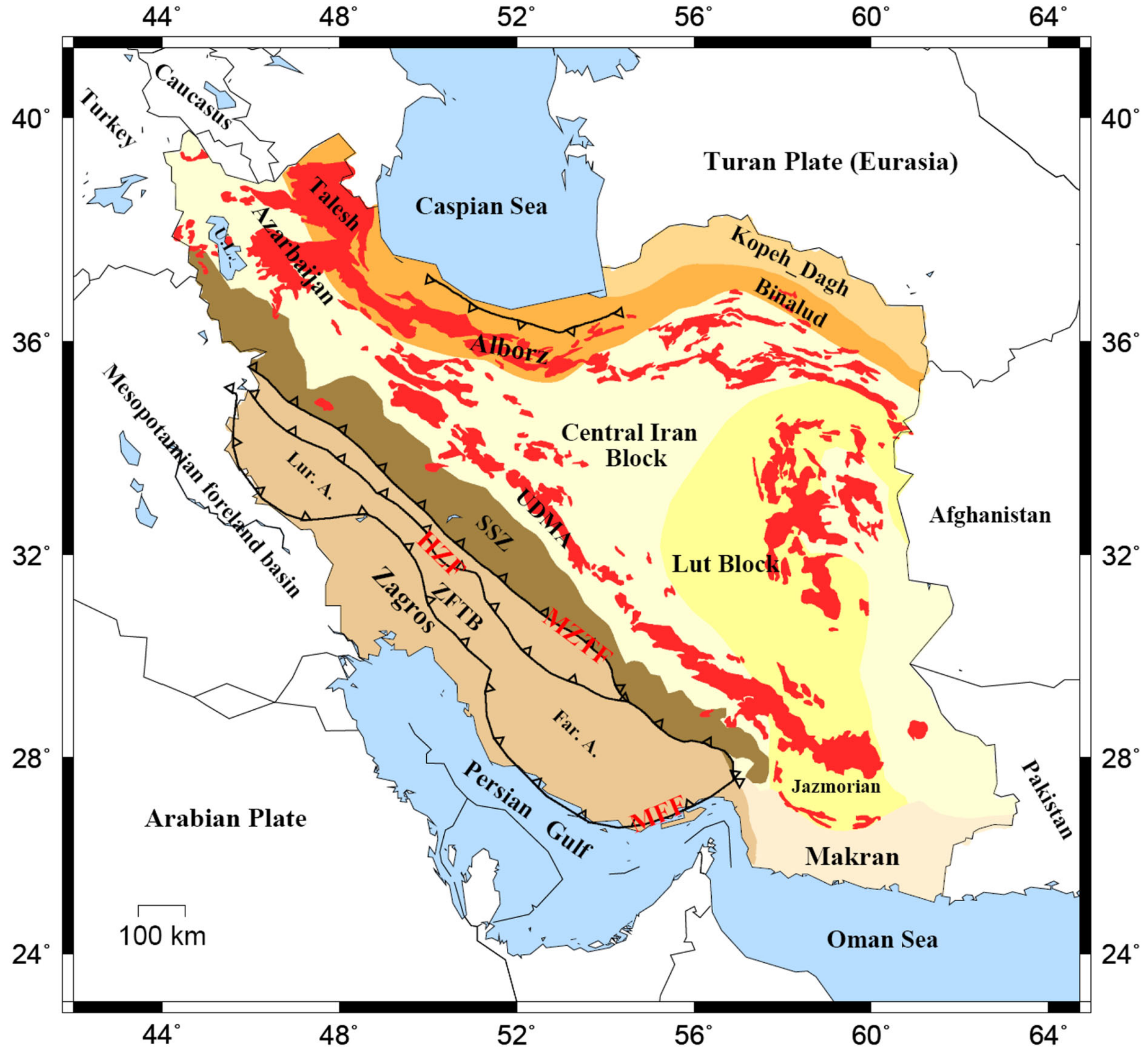

Figure 1

Different tectonic units of the Iranian plate. *UL* Urumieh Lake, *SSZ* Sanandaj-Sirjan Zone, *ZFTB* Zagros Fold and Thrust Belt, *MZTF* Main Zagros Thrust Fault, *HZF* High Zagros Fault, *MFF* Main Front Fault, *UDMA* Urumieh–Dokhtar Magmatic Arc, *Lur. A.* Lurestan Arc; *Fars A.* Fars Arc. Faults are from Jiménez-Munt *et al.* (2012)

tectonic evolution of the region. The complex tectonic structure of Iran provides an ideal study area for investigation of crustal thickness. A large number of studies have focused on the crustal structure and have shown the topography of the Moho discontinuity beneath different parts of Iran (e.g. Asudeh, 1982; Javan Doloei and Roberts, 2003; Hatzfeld *et al.*, 2003; Sodoudi *et al.*, 2009; Paul *et al.*, 2006, 2010; Taghizadeh-Farahmand *et al.*, 2010, 2013; Radjaee *et al.*, 2010; Abbassi *et al.*, 2010; Afsari *et al.*, 2011, Mohammadi *et al.* 2013a). However, they were mostly limited to the narrow profiles and could not cover the whole Iran.

Dehgani and Makris (1984) constructed the first Moho depth map of Iran from Bouguer anomaly modeling and seismic data. This map has been often used as the only reference Moho depth map for Iran.

Currently, due to the growing number of national Iranian seismological networks and large amounts of available data, a more accurate Moho depth map is required.

The main goal of this paper is to resolve the Moho discontinuity and its lateral depth variations beneath different tectonic zones of Iran using all Iranian broadband and short-period stations for the first time. We calculate the P receiver functions beneath each station and apply the Zhu and Kanamori method (Zhu and Kanamori, 2000) (Z&K) as well as 1-D forward modeling to map the topography of the Moho boundary with a higher resolution (error of ±2 km) than that previously presented.

2. Data and Analysis

The data used for this study were recorded by the Iranian Telemetry Seismic Networks (ITSN), which consists of 11 seismic networks with 53 permanent short-period seismic stations. In addition, we used the data of 24 broadband stations (Fig. 2). The short-period networks are operated by the Iranian Seismological Center (ISC). They are equipped with SS-1 seismometers with a natural frequency of 1 Hz made by Nanometrics and are connected to the central recording station via a telemetric system. The broadband stations operated by the International Institute of Earthquake Engineering and Seismology (IIEES) are equipped with three component Güralp (CMG-3TD) sensors. Names of the networks and stations and their geographical coordinates are listed in Table 1. Teleseismic data, which were recorded between 1995 and 2011, have been used in this study. More than 1,400 teleseismic events (Fig. 3) with magnitudes greater than 5.5 (Mb) at epicentral distances between 30° and 95° have been used for the P Receiver Function (PRF) analysis. The methodology for PRF analysis used in this paper is the same as described by Yuan *et al*. (1997).

Calculation of PRFs is performed in three different steps including removal of the instrument response, coordinate rotation into the local LQT ray-based coordinate system (as described by Vinnik, 1977), and deconvolution in time domain (as described by Kind *et al*., 1995), which results in having the converted P-to-S phases on the Q component. A reference slowness of 6.4 s/° is considered for the moveout correction. PRFs are then stacked and filtered with a low-pass filter of 2 s (Butterworth, three poles).

Another step often employed in receiver function analysis is inversion, which can find the most suitable average shear wave velocity and crustal thickness beneath each seismic station. However, unreliable results will occur if no clear converted phases or multiples exist in the time domain receiver functions. In such cases, seismic noise may be transformed into a velocity-depth model. Therefore, we prefer forward modeling (inversion with additional parameters) of the receiver functions (e.g. Kumar *et al*., 2007). This procedure is more realistic than a blind automatic inversion without phase identification. For this reason, we first identified the Moho conversion in the data, which is often the largest phase on the Q component. Other phases, which are frequently detected in time domain receiver functions are conversions from the bottom of sedimentary layers and crustal multiples. We picked the arrival times of all these phases. A grid search was then performed to find a crustal model, which fits the waveforms reasonably well. For each tectonic zone, we used appropriate velocity models inferred by previous studies (Table 2).

3. P Receiver Function Observations

Teleseismic events with a relatively high signal-to-noise ratio (larger than 4) have been selected for most of the stations. This criterion significantly reduced the number of PRFs beneath each station. For stations with a relatively high noise level, a large number of data must be deleted (e.g. BJRD). Figure 4 shows individual and stacked PRFs for some short-period (MHD and VIS) and broadband stations located in different tectonic zones. PRFs are sorted by increasing back azimuth. The stacked PRFs (at the top of the Fig. 4) reliably show a clear Ps conversion from the Moho ranging between 4.8 and 6.4 s. This conversion can be clearly followed in the individual traces. Other phases detected in the receiver functions are related to the conversions from the bottom of

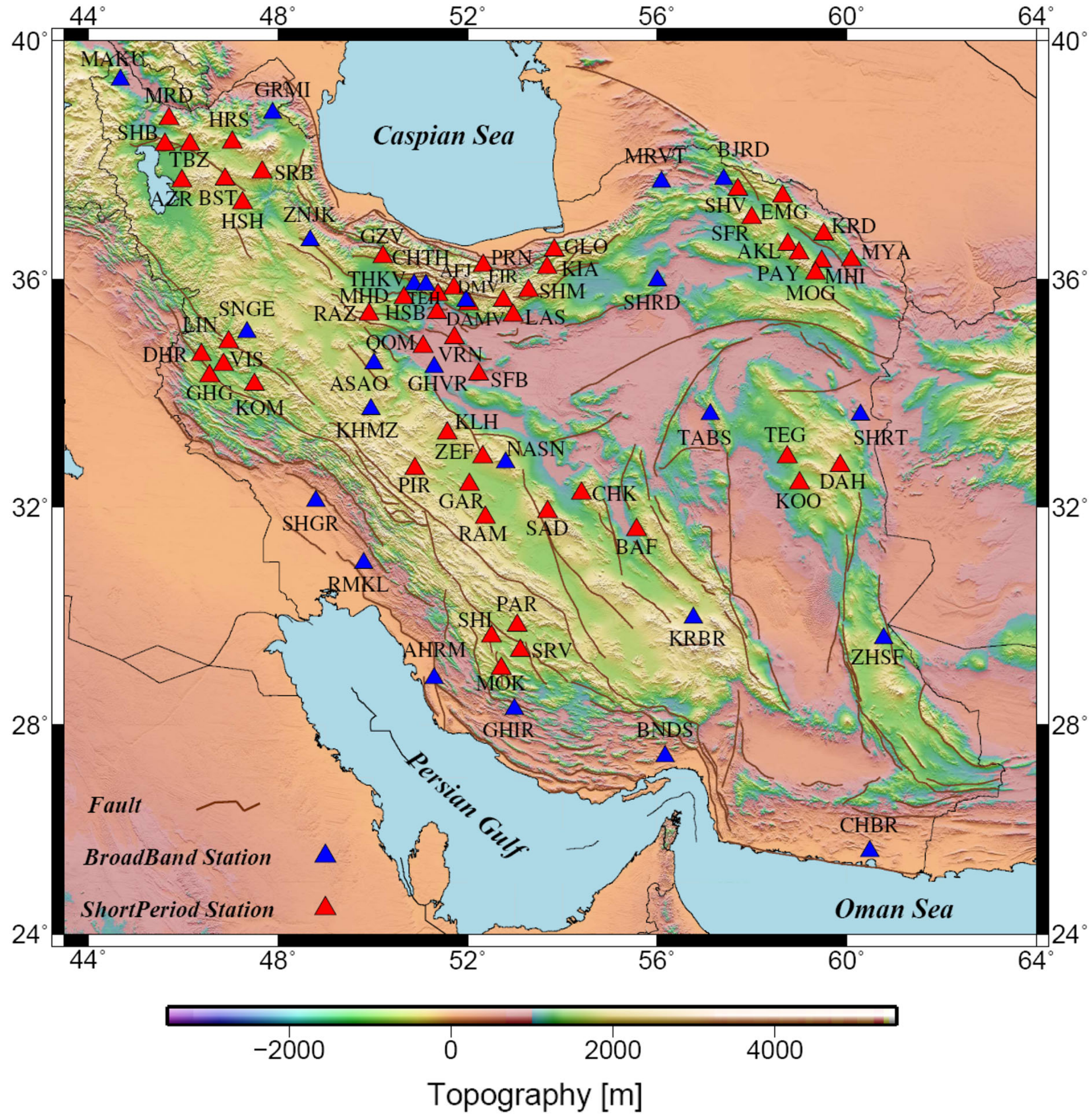

Figure 2
Location map of the seismological stations used in this study. Stations are shown with red (short period) and blue (broadband) triangles. Active faults are shown with brown lines (Hessami *et al*., 2003)

sedimentary layers and crustal multiples. The minimum arrival time of the Moho converted phase (3.7–3.8 s) is observed beneath the stations CHBR and RMKL located in the southeastern and southwestern part of Iran, respectively. However, the largest arrival time (8.0 s) is seen beneath the station KHMZ located in the SSZ. The stacked PRFs at all stations in different tectonic zones are presented in Fig. 5a–e and arranged after the Moho phase arrival time in seconds. The arrival time of the Moho converted phase can be clearly seen in the PRF data. Small differences in the arrival time of the Moho-converted phase can be observed in some tectonic zones (e.g. Kopeh-Dagh, Alborz). Beneath the Zagros

Table 1

Specification of the seismic stations, Ps conversion times (s), Moho depths (km) and number of PRFs

Code Station	Geographical Coordinates			Ps Moho Time (s)	Moho Depth (±2,km) Ps time	Moho Depth (km) Z&K	Moho Depth (±2 km) Modeling	No of PRFs
	Latitude (°)	Longitude (°)	Altitude (m)					
(A)								
ASAO	34.548	50.025	2217	6.8	52.0	–	52	83
GHVR	34.480	51.295	927	4.7	36.0	37.5 ± 1.0	42	45
KHMZ	33.739	49.959	1985	8.0	61.0	64.5 ± 2.0	66	27
SHGR	32.108	48.801	150	6.1	46.5	47.0 ± 1.0	46	19
TABS	33.649	57.119	1106	5.8	44.0	44.0 ± 1.2	44	26
RMKL	30.982	49.809	176	3.7	32.0	–	42	5
AHRM	28.864	51.295	80	4.2	36.0	–	42	5
CHTH	35.908	51.126	2350	5.5	46.0	49.5 ± 1.5	55	31
DAMV	35.630	51.971	2520	6.9	57.5	52.5 ± 2.0	56	93
THKV	35.916	50.879	1795	7.0	58.0	52.0 ± 1.5	56	79
SHRT	33.646	60.291	837	5.0	42.0	38.0 ± 1.5	42	27
KRBR	29.982	56.761	2576	5.0	42.0	38.0 ± 1.2	42	69
BNDS	27.399	56.171	1500	7.2	60.0	55.0 ± 1.5	53	58
ZNJK	36.670	48.685	2200	5.5	46.0	45.5 ± 2.0	47	25
MRVT	37.659	56.089	870	6.0	45.0	42.0 ± 1.0	45	59
SHRD	35.99	56.01	1264	5.5	45.0	44.0 ± 1.5	45	5
BJRD	37.700	57.408	1337	6.5	49.0	49.5 ± 1.2	49	23
MAKU	39.355	44.683	1730	4.4	38.0	41.5 ± 1.0	42	73
GRMI	38.810	47.894	1300	4.4	38.0	37.0 ± 3.0	41	35
GHIR	28.286	52.987	1200	5.9	50.0	47.0 ± 2.0	47	54
SNGE	35.093	47.347	1940	4.7	41.0	45.0 ± 1.5	42	58
NASN	32.799	52.808	2379	6.6	53.0	56.5 ± 2.0	56	65
CHBR	25.595	60.482	125	3.7	32.0	31.5 ± 1.5	33	7
ZHSF	29.611	60.775	1575	5.1	43.0	44.0 ± 1.5	43	45

Net.	Code Station	Geographical Coordinates			Ps Moho Time (s)	Moho Depth (±2 km) Ps time	Moho Depth (km) Z&K	Moho Depth (±2 km) Modeling	No of PRFs
		Latitude (°)	Longitude (°)	Altitude (m)					
(B)									
Tabriz	AZR	37.6772	45.9828	2270	5.5	46.0	47.0 ± 0.5	46	54
	BST	37.7004	46.8889	2110	5.3	44.5	42.5 ± 1.0	44	38
	HSH	37.3053	47.2636	2142	5.6	47.0	46.0 ± 1.0	45	15
	HRS	38.3173	47.0433	2112	5.9	49.5	49.0 ± 1.0	49	23
	MRD	38.7133	45.703	2150	6.2	52.0	52.0 ± 0.5	50	70
	SHB	38.2833	45.6166	2298	5.0	42.0	39.0 ± 1.2	38	35
	SRB	37.823	47.668	2020	6.6	55.5	53.5 ± 1.0	53	28
	TBZ	38.2348	46.1499	1583	5.1	43.0	46.0 ± 1.0	44	41
Kermanshhah	DHR	34.6991	46.389	1811	4.6	39.0	36.0 ± 1.0	40	21
	KOM	34.1762	47.5143	1714	4.6	39.0	39.0 ± 1.0	41	42
	GHG	34.3293	46.5684	2061	5.4	46.0	42.0 ± 1.0	44	22
	LIN	34.9187	46.9626	2139	4.5	38.0	37.0 ± 1.0	40	14
	VIS	34.5275	46.8511	1828	5.9	50.0	51.5 ± 1.0	50	35
Isfahan	PIR	32.6841	50.8917	2550	5.2	44.0	40.5 ± 1.0	42	42
	GAR	32.4063	52.0474	1910	7.1	60.5	56.0 ± 1.0	55	7
	KLH	33.319	51.5787	2157	4.7	40.0	42.5 ± 1.5	42	34
	ZEF	32.8956	52.3291	2321	6.6	56.0	50.0 ± 1.5	46	20
	RAM	31.7983	52.3827	2198	6.0	51.0	53.5 ± 2.0	52	11
Yazd	BAF	31.59	55.567	1414	5.5	46.0	44.5 ± 1.5	44	22
	CHK	32.2438	54.4079	1533	4.4	37.0	39.0 ± 1.0	42	23
	SAD	31.9133	53.6854	2461	6.5	54.0	51.5 ± 2.0	50	5

Table 1

continued

Net.	Code Station	Geographical Coordinates			Ps Moho Time (s)	Moho Depth (±2 km) Ps time	Moho Depth (km) Z&K	Moho Depth (±2 km) Modeling	No of PRFs
		Latitude (°)	Longitude (°)	Altitude (m)					
Birjand	TEG	32.8967	58.7489	1713	5.4	41.0	40.0 ± 1.5	40	88
	DAH	32.7386	59.8677	2328	4.7	36.0	38.5 ± 1.3	39	68
	KOO	32.4241	59.0044	1928	5.4	41.0	44.0 ± 1.3	42	93
Semnan	LAS	35.3802	52.9595	1449	6.6	54.0	50.0 ± 1.0	52	65
	SHM	35.8064	53.2841	2633	7.7	63.0	60.0 ± 1.0	62	53
Sari	GLO	36.5027	53.8301	1930	6.0	50.0	45.5 ± 1.5	50	82
	KIA	36.207	53.6837	2153	6.4	53.0	50.5 ± 1.0	52	89
	PRN	36.2419	52.3381	1304	6.0	50.0	47.0 ± 1.0	52	12
Tehran	TEH	35.74	51.385	1371	6.2	51.5	51.0 ± 2.0	53	10
	AFJ	35.856	51.7125	2761	6.2	51.5	47.5 ± 2.0	48	57
	FIR	35.6415	52.7536	2374	6.3	52.5	55.0 ± 1.5	54	114
	GZV	36.3859	50.2184	2451	6.8	56.5	48.0 ± 2.0	46	77
	DMV	35.5772	52.0322	2498	7.8	65.0	57.5 ± 1.0	57	114
	SFB	34.3509	52.2464	975	6.3	52.5	48.0 ± 2.0	47	36
	VRN	34.9953	51.7275	1138	6.4	53.0	49.0 ± 3.0	50	91
	MHD	35.6851	50.6674	1659	6.4	53.0	48.5 ± 1.5	49	48
	HSB	35.4378	51.2757	1119	6.0	50.0	52.5 ± 2.0	49	112
	RAZ	35.4044	49.9292	1940	6.1	51.0	47.5 ± 2.0	49	94
	QOM	34.8416	51.0627	1000	5.6	47.0	47.5 ± 2.5	45	74
Shiraz	SHI	29.6371	52.5202	15964	5.8	49.0	51.5 ± 1.1	48	25
	SRV	29.3817	53.1133	2625	5.7	48.0	49.5 ± 1.3	47	68
	MOK	29.0461	52.7146	2755	5.5	46.5	47.0 ± 1.2	48	87
	PAR	29.8404	53.0481	2576	6.6	56.0	56.0 ± 1.3	54	32
Mashhad	MYA	36.3416	60.1017	1671	4.8	40.0	40.0 ± 2.0	43	45
	KRD	36.776	59.5146	2245	5.5	46.0	42.0 ± 1.5	45	34
	PAY	36.4542	58.9904	2014	5.4	45.0	48.0 ± 2.0	45	38
	MOG	36.108	59.3391	2575	5.5	46.0	47.5 ± 1.2	46	32
	MHI	36.309	59.4705	1169	5.6	46.5	50.0 ± 1.0	49	23
Quchan	AKL	36.5946	58.7542	2507	5.8	48.0	44.0 ± 1.0	47	26
	EMG	37.408	58.6512	2539	5.8	48.0	45.0 ± 2.0	46	32
	SFR	37.0436	58.0022	2223	6.2	51.5	50.0 ± 1.0	48	40
	SHV	37.5333	57.696	1909	6.3	52.5	49.0 ± 1.5	49	11

(A) Broadband Stations, (B) Short-Period Networks

zone and Central Iran these differences seem to be relatively larger. This led us to divide these zones into subregions. Based on our observations, the Moho-converted phase is seen at delay times ranging between 4.8 and 6.5 s beneath the Kopeh-Dagh. It is observed at 5.5–7.8 s delay times beneath the Alborz zone. We found relatively smaller delay times for the Moho phase beneath Central Iran (4.4–6.6 s) and Makran zone (3.8 s). The delay time of the Moho-converted phase ranges between 3.7 and 6.8 beneath Zagros. The largest delay time of the Moho phase is seen beneath the SSZ (station KHMZ, 8 s).

4. *Crustal Thickness*

We estimated Moho depths based on Ps conversion times using available velocity models obtained from the previous geophysical studies in Iran for each tectonic zone (see Table 2). The Moho depths are listed in Table 1. The Moho depth varies between 32 ± 2 km at CHBR station in the Makran zone and 61 ± 2 km at KHMZ station in the SSZ. In the next step, we have used the arrival times of crustal multiples to determine the crustal thickness using the Z&K stacking approach. We

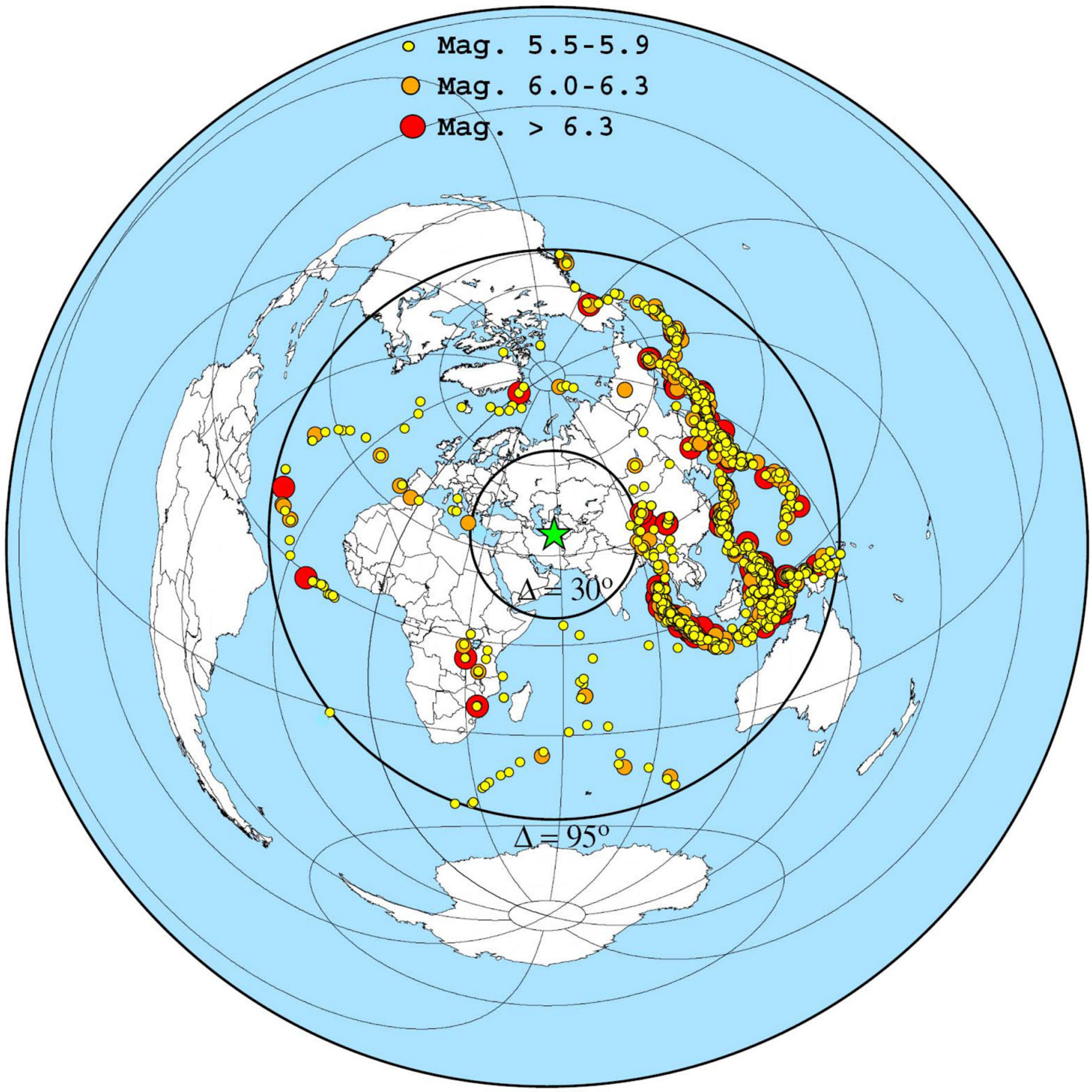

Figure 3
Distribution of teleseismic events recorded by the national permanent stations of Iran between 1995 and 2011 and used to calculate P receiver functions. The *green star* represents the approximate position of Iran. The *black solid circles* mark the 30° and 95° epicentral distances, respectively

applied this method only for stations which show clear multiple phases. We chose weight factors of 0.5, 0.25, and 0.25 for Moho conversion and crustal multiples, and performed a grid search for estimating the Moho depth and crustal Vp/Vs ratio. The maximum amplitude of stacked traces occurs where the three phases add constructively. The results of the Z&K method for some stations (shown in Fig. 4) are presented in Fig. 6. We also show the stacked moveout corrected receiver functions for the Ps and the multiple phases (PpPs and PpSs), respectively. As Fig. 6 shows the multiple phases are amplified after the correct moveout correction and fit the arrival times predicted by the final model. The Moho depths obtained from the Z&K method are also listed in Table 1. Based on

Table 2

Different velocity model that are used as reference in different tectonic zone in this study

Tectonic zone	Velocity model
Alborz	Abbassi *et al.* (2010)
Kopeh-Dagh	Motaghi *et al.* (2012)
Zagros	Paul *et al.* (2010); Hatzfeld *et al.* (2003); Afsari *et al.* (2011)
Makran	Shad Manaman *et al.* (2011)
Central_Iran	Paul *et al.* (2010); Taghizadeh-Farahmand *et al.* (2010); Zamanian *et al.* (2012); Azhari *et al.* (2012)

our finding, the Moho depth varies between 31.5 ± 1.5 km at station CHBR in the Makran zone and 64.5 ± 2 km at station KHMZ in the SSZ. At some stations with very weak multiples, we found relatively large differences between the estimated Moho depths obtained from the Ps arrival time and Z&K method (see Table 1).

5. P Receiver Function Modeling

We used forward modeling of the receiver functions to find the most suitable crustal thickness beneath each station (see also Taghizadeh-Farahmand *et al*. 2010 and Afsari *et al*., 2011). P wave velocity models shown in Table 2 were used as starting models for each tectonic zone. Figures 7 and 8 illustrate the results of forward modeling for one short-period (MHD) and one broadband station (SNGE) (see also Fig. 4). We first determined the Moho depth and tried to find the simplest model, which fits all other converted phases (e.g. sedimentary layers, Moho multiples). As an example, we present in Figs. 7 and 8 three selected models among many other models calculated for stations MHD and SNGE. A simple model containing a pronounced sedimentary layer and a Moho boundary can be well matched with the observed seismograms. Moho depths obtained from forward modeling are listed in Table 1. We also showed the differences between the results of forward modeling and those obtained from Ps arrival time in Fig. 9. In general, the differences are not larger than 4 km (except nine stations).

6. Results and Discussion

We presented new Moho depth maps for Iran derived from our results of Ps arrival time, Z&K approach, and forward modeling (Fig. 10a-c). To construct the Moho depth map we interpolate all the depth values directly obtained from our analysis beneath stations. Our interpolation is reliable for the areas, which are well covered by stations (e.g. western Iran). This is in contrast to some other areas (e.g. Central Iran), where our estimations are limited to the results of few stations. For these areas, the depth values beneath each station are also shown with colors and are more accurate than those obtained from the linear interpolation. All our three Moho depth maps reveal the same trend beneath Iran, implying that the thickest crust is beneath the Alborz zone and along the SSZ zone. While the crustal thickening beneath the Alborz is related to the shortening process associated with the orogenic belt, the crustal thickening beneath the SSZ may reveal the underthrusting of the Arabian plate beneath the Iranaian plate (Paul *et al*., 2010; Mohammadi *et al.* 2013a). The average crustal thickness elsewhere in Iran is about 40-45 km except in southeast Iran which shows a normal continental crust of about 33 ± 2 km, which has not been significantly influenced by collisional processes.

Our presented Moho depth map (from PRF modeling, Fig. 10c) is the first Moho depth map obtained from high frequency receiver functions and appears to be more accurate (error of ±2 km) than the global Moho depth maps (e.g. Mooney *et al*., 1998; Bassin *et al*., 2000), which provide rough estimates of the Moho depth within Iran and those previously obtained by gravity data (Dehgani and Makris 1984), partitioned waveform inversion (Shad Manaman *et al*., 2011) and regional/residual Bouguer anomalies (Jiménez-Munt *et al*., 2012). In the following subsections, we summarize and compare our results obtained from modeling for each tectonic zone of Iran with those shown by previous geological and geophysical studies.

6.1. The Caspian Basin and Surrounding Mountain Ranges (Alborz, Binalud, and Kopeh-Dagh)

The Alborz mountains form a seismically active fold-and-thrust belt along the southern Caspian Sea

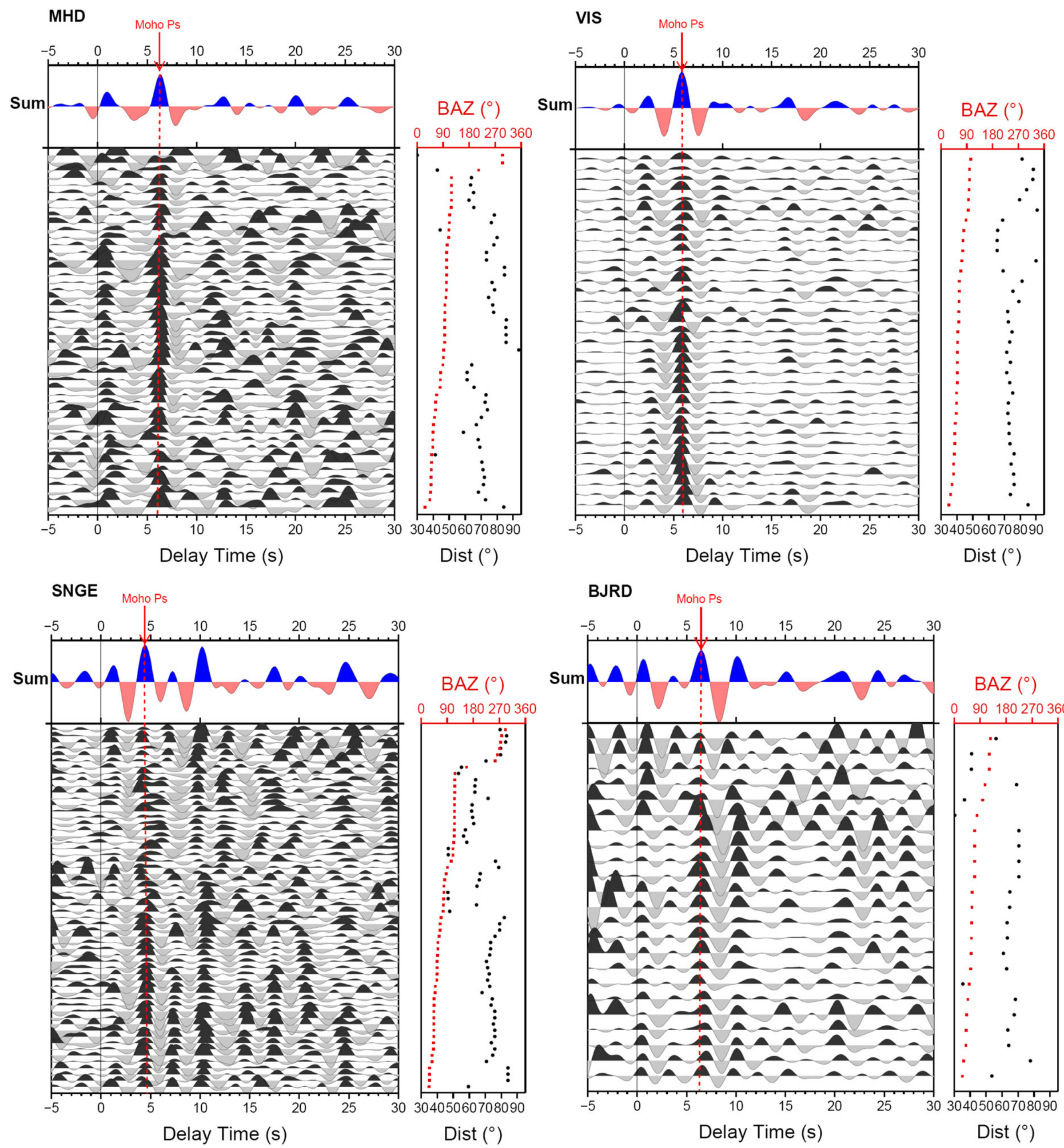

Figure 4

Individual PRFs with summation traces for seven broadband and two short-period stations (MHD, VIS) in different tectonic zones of Iran. Individual seismograms are plotted equally spaced and sorted by increasing back azimuth (*red rectangles*). *Black dots* indicate the epicentral distances (shown on the *right*). They are filtered with a low-pass filter of 2 s. The P onset is fixed at zero time. The Ps conversion phases from the Moho are marked with *red dashes lines* (labeled Moho Ps)

coast extending from the southern end of the Talesh Mountains in the west to their junction with the Kopeh-Dagh Mountains in the east and central Iran in the south (Fig. 1). A number of geophysical studies have focused on the crustal structure of the Alborz region (e.g. Sodoudi *et al*., 2009; Abbassi *et al*., 2010; Radjaee *et al*., 2010; Motavalli-Anbaran *et al*., 2011; Nasrabadi *et al*., 2011) and provided different

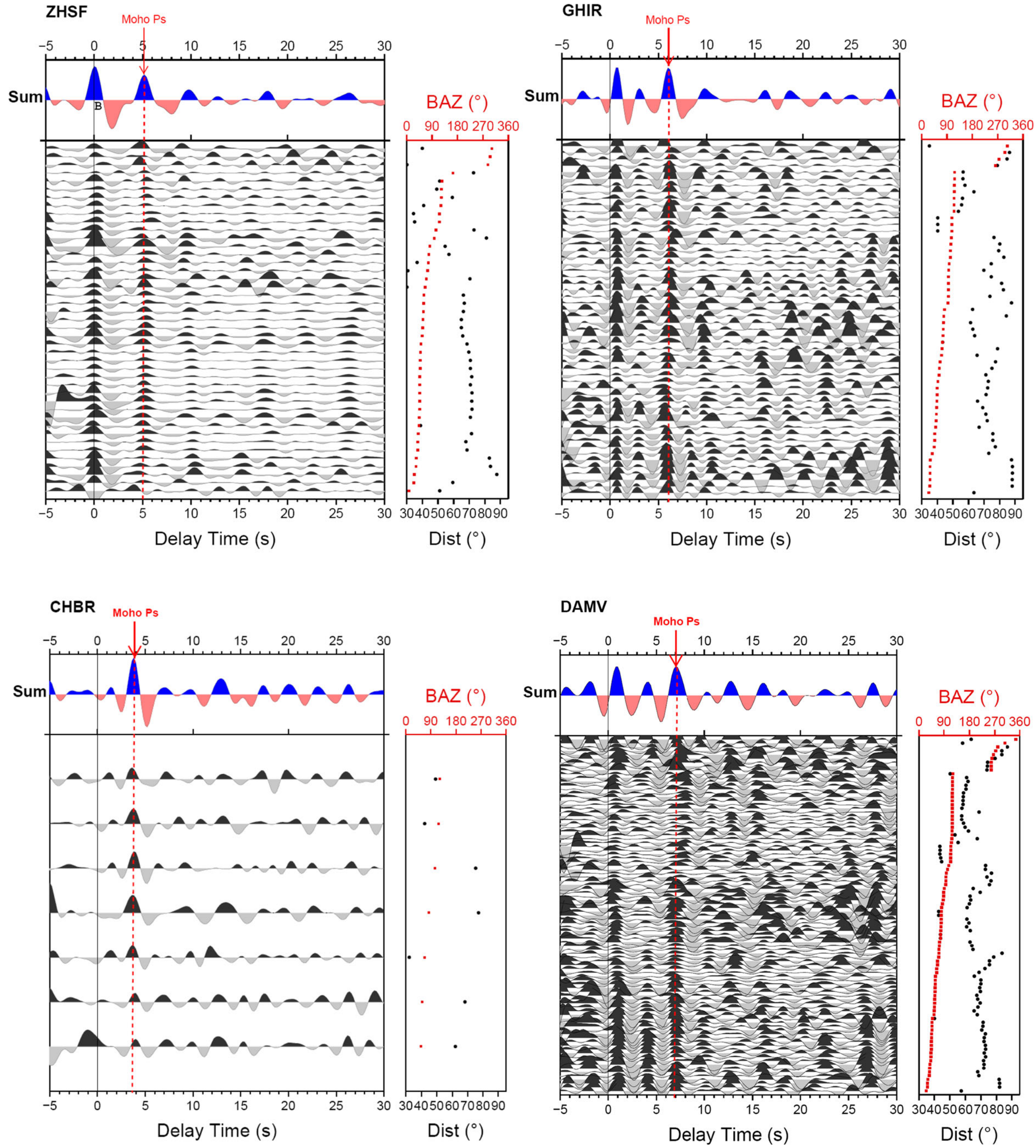

Figure 4
continued

estimates of the Moho depths due to various assumed body wave velocities and model resolutions. Our results showed a thickening of the crust from 47 ± 2 km beneath the western part of the Alborz mountains (station ZNJK) to ~54 ± 2 km below the central part of this region. Beneath the southeastern part of the Alborz mountains in the Binalud zone, the crust thins out and is 45 ± 2 km thick (station

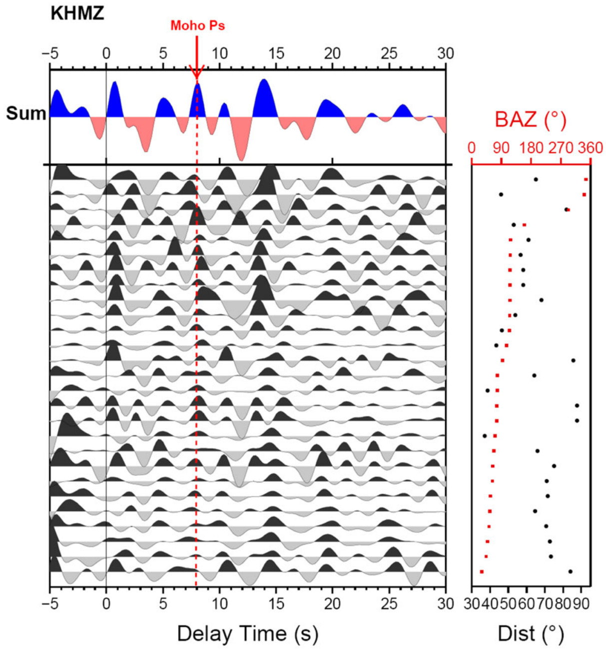

Figure 4
continued

SHRD). We also observed a decrease in the Moho depth towards the north and south of central Alborz. A crustal thickness of ∼51–54 km was shown by the joint analysis of P and S receiver functions beneath the central Alborz by Sodoudi *et al*. (2009). They found an unusual crustal thickness of about 67 km beneath the Damavand volcano, which is located on southern flank of the range. However, their analysis was based on the data obtained from one short period station (DMV). Moreover, they used the IASP91 reference model (Kennett and Engdahl, 1991) for the depth estimation, which may have higher crustal velocities than the local model used in this work. Our results revealed a relatively large crustal thickness beneath the Alborz region, which can be related to the shortening process. A local crustal thickening to about 57 ± 2 km beneath the central part of Alborz (obtained from three stations, DMV and DAMV and THKV) is consistent with the result of Sodoudi *et al*. (2009) beneath the Damavand volcano if we take the errors of depth estimation produced by using a reference model into account (∼5 %). This local thick crust may be attributed to the magmatic addition at the base of the crust beneath the volcanic region (Sodoudi *et al*., 2009). If it is valid, we may confirm the earlier suggestions (e.g. Dehgani and Makris 1984; Jackson *et al*., 2002) showing no deep root beneath the high-elevated central Alborz. Our findings are also consistent with the results shown by joint inversion of receiver functions and Rayleigh wave group velocity (Abbassi *et al*., 2010; Nasrabadi *et al*., 2011), and those obtained from fundamental mode Rayleigh wave group velocities (Radjaee *et al*., 2010).

Beneath Kopeh-Dagh we estimated an average crustal thickness of about 45 ± 2 km. Furthermore, we showed that the Moho depth varies from ∼43 ± 2 km beneath the southern Kopeh-Dagh foreland basin to ∼49 ± 2 km below the northern part of the basin. Our results can be confirmed by those obtained by Mangino and Priestley (1998) and Jiménez-Munt *et al*. (2012) for the NE Iran. They are also in good agreement with those shown by Motavalli-Anbaran *et al*. (2011), who estimated the Moho depths using gravity, geoid, topography, and surface heat flow data.

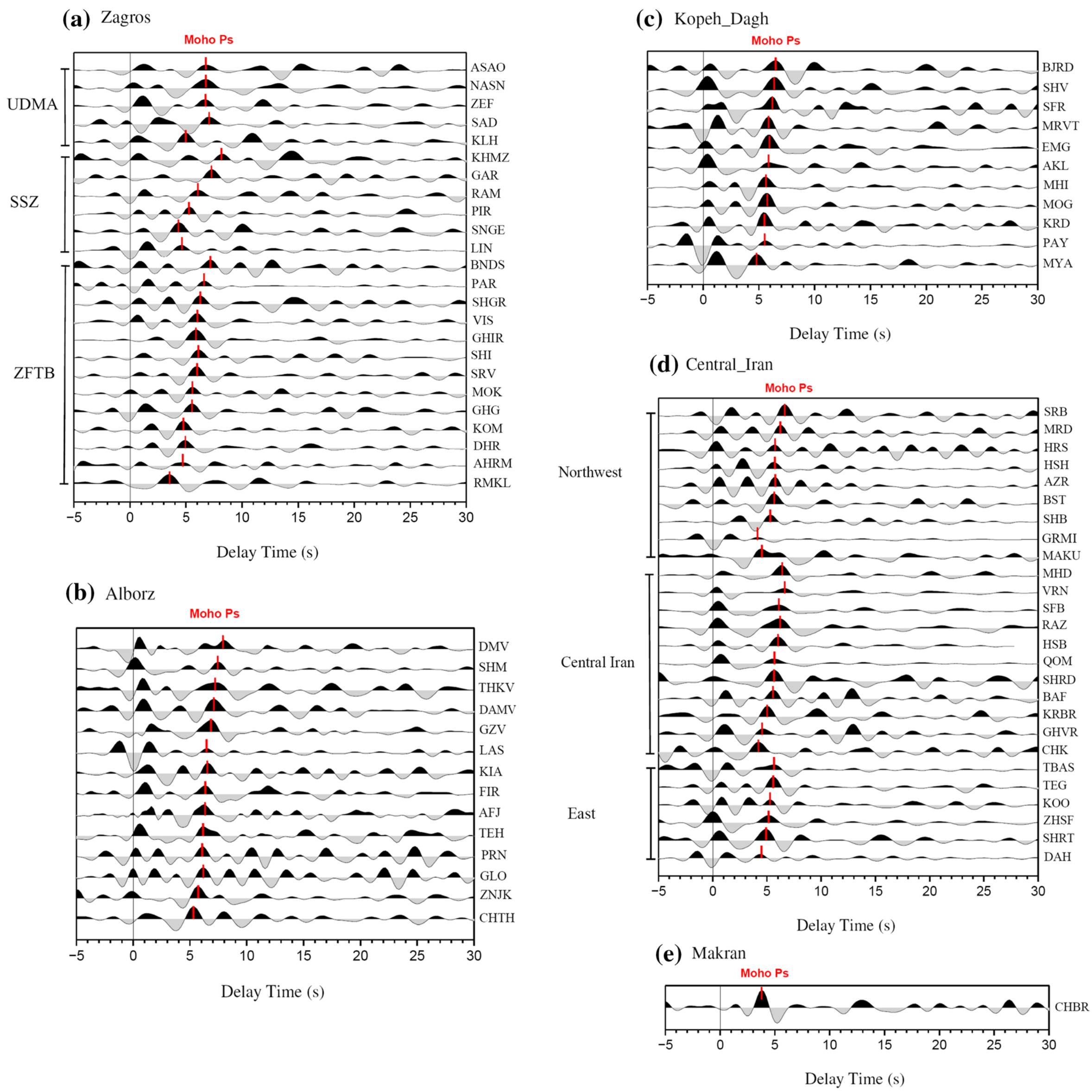

Figure 5

Stacked PRFs obtained for each tectonic zone. A low-pass filter of 2 s is applied. PRFs are sorted by the increasing arrival time of the Moho converted phase. Ps conversions from the Moho discontinuity are shown by *red bar lines* (labeled Moho Ps). **a** Stacked PRFs for stations located in the Zagros orogenic system (ZFTB, SSZ and UDMA). **b** Same as (a) for the Alborz tectonic zone. **c** Same as **a** for the Kopeh-Dagh mountain range. **d** Same as **a** for Central Iran. **e** Same as **a** for the Makran subduction zone

6.2. The Zagros Orogenic System

The Zagros Mountain belt in southwestern Iran results from the collision of Arabia and Eurasia plates most likely in the early Miocene. Previous studies in the Zagros (e.g. gravity and seismic studies) indicated a relatively thick crust (∼40–45 km) beneath this region (Snyder and Barazangi 1986; Hatzfeld *et al*. 2003; Paul *et al*. 2006; Shad Manaman and Shomali 2010; Afsari *et al*. 2011; Mohammadi *et al*. 2013). We that found various Moho depths related to the different structure units exist in this area. According to our results (Fig.10c), the crust has an average thickness of about 43 ± 2 km beneath the NW Zagros Fold and Thrust Belt (ZFTB, Fig. 1) and

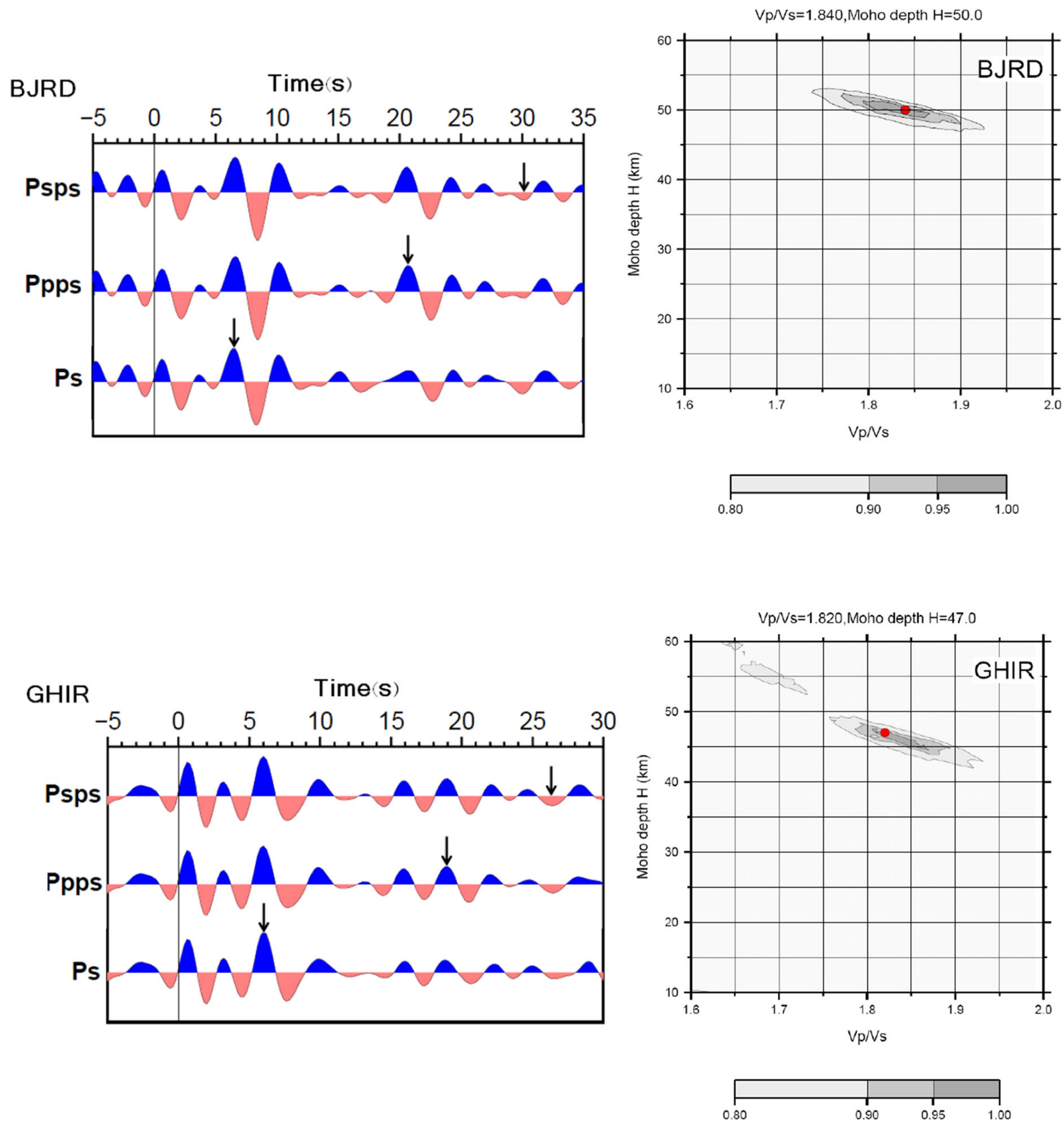

Figure 6

Examples of Z&K stacks of receiver functions for six stations indicated also in Fig. 4. A grid search is performed to estimate the Moho depth and crustal Vp/Vs ratio. The amplitude is shown in the lower part and ranges from 0.8 to 1. The optimal combination of the crustal thickness and Vp/Vs ratio is defined where the largest amplitude (1) occurs as marked by a red solid circle. The three traces on the left side of each panel show receiver functions after moveout correction for the Ps, PpPs, and PpSs phases, respectively. Black arrows mark the predicted times of the three phases obtained from the grid search

shows a significant thickening ($\sim 51 \pm 2$ km) beneath the central part of this region, which most likely represents the overthrusting system beneath this area (Berberian 1995). This result is consistent with that shown by Afsari *et al*. (2011). The average Moho depth increases to about 48 ± 2 km below the central part of the ZFTB. At the end of the SE Zagros between the Zagros continental collision and Makran

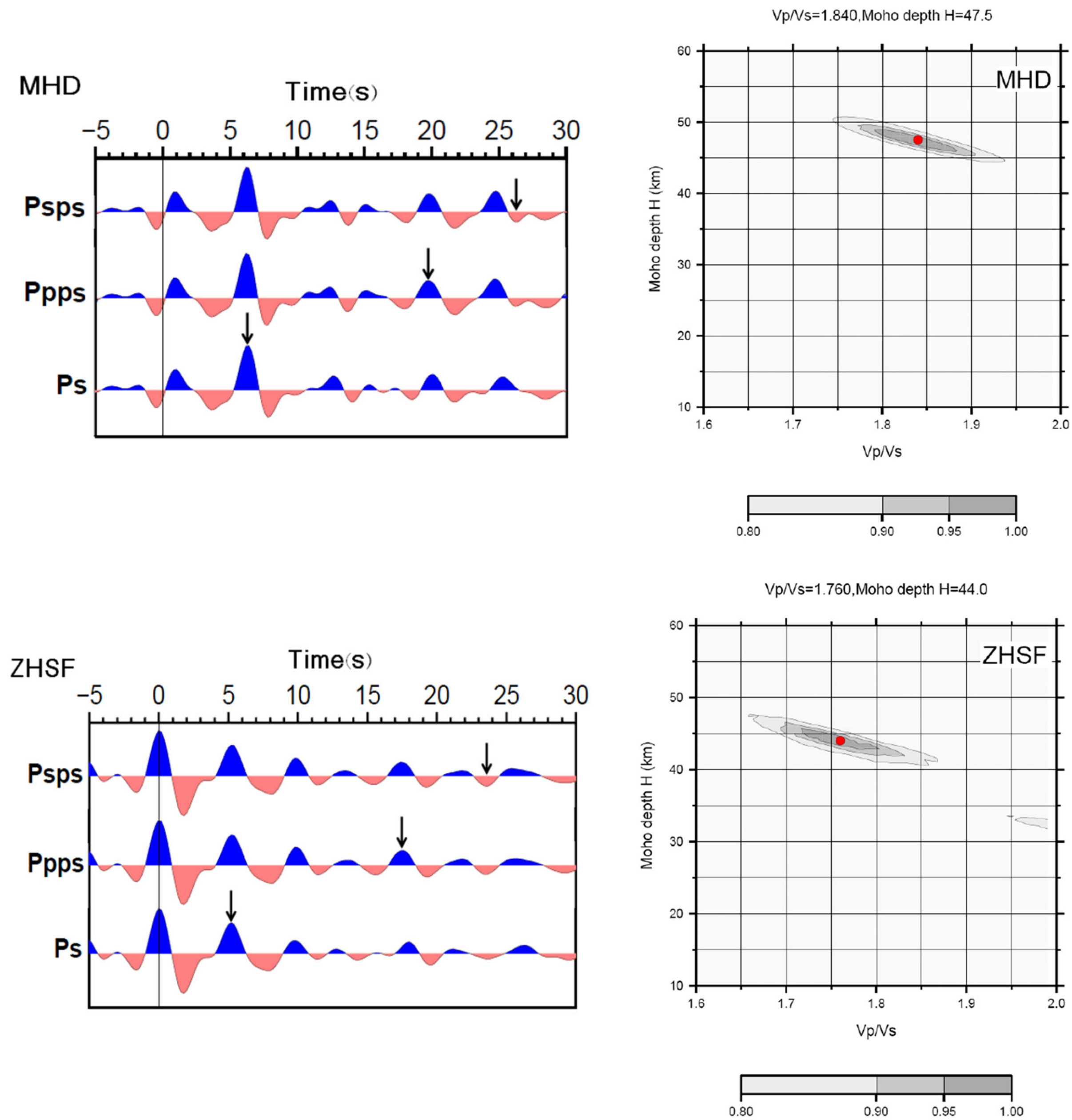

Figure 6
continued

subduction zone, our Moho depth map indicates a crustal thickness of about 52 ± 2 km confirming the results shown by Yamini-Fard and Hatzfeld (2008) and Tatar and Nasrabadi (2013). In general, our Moho depths are consistent with those obtained from other studies in the ZFTB (e.g. Hatzfeld *et al.*, 2003; Paul *et al.*, 2006; 2010). Our results indicate that crustal thickening and shortening in the collision zone of Zagros is not constant. These results are consistent with those shown by Vernant *et al.* (2004) and Vernant and Chéry (2006), who indicated that the convergent rate varies from 4.5 ± 2 mm year^{-1} in the northwestern part, to 9 ± 2 mm year^{-1} in the southeastern part of the Zagros.

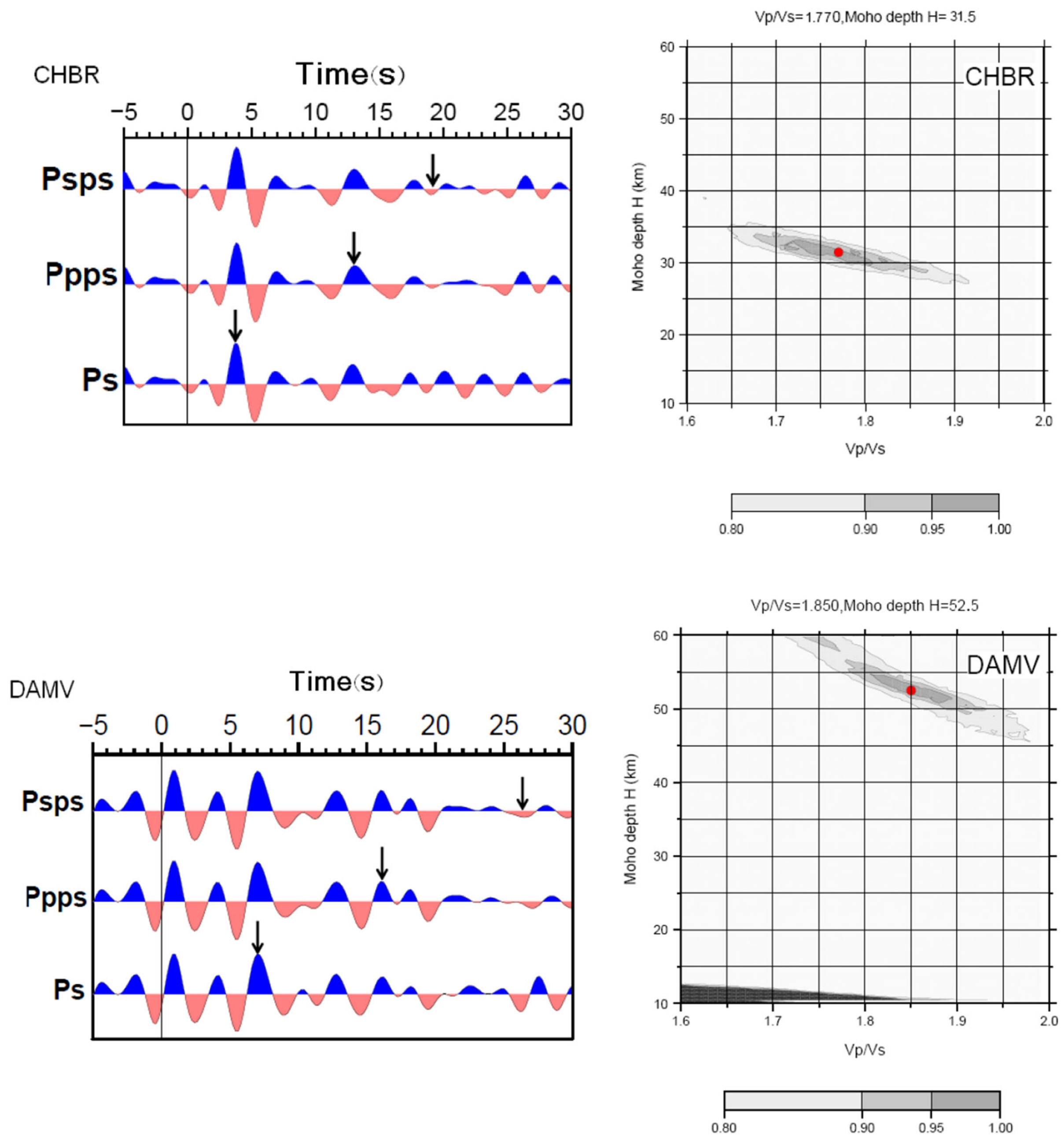

Figure 6
continued

Beneath the SSZ we observe an average crustal thickness of about 54 ± 2 km with a strong increase to about 66 ± 2 km (beneath KHMZ). Paul *et al.* (2010) compared the Bouguer anomaly data and the Moho depths obtained from two profiles crossing the ZFTB and the SSZ. Their comparison significantly showed that the location of the maximum Moho depth beneath the SSZ does not coincide with the minimum Bouguer anomaly. To reconcile the gravity data with Moho depths they proposed that the localized thickening beneath the SSZ reveals the overthrusting of the crust of Central Iran onto the

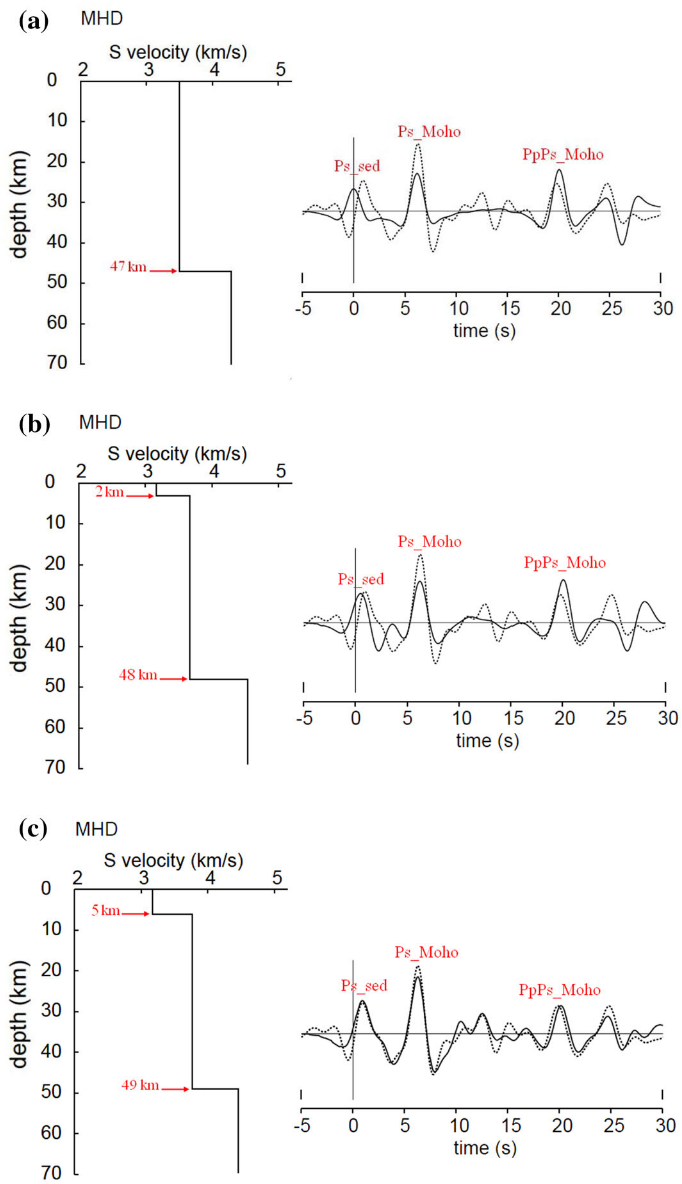

Figure 7

Forward modeling of the stacked PRF for station MHD located in Central Iran. The *dashed line* in the right panel is the observed P receiver function. The *solid line* represents the synthetic P receiver function corresponding to the model shown in the left. **a** Synthetic PRF calculated for a model with a Moho boundary at 47 km depth. **b** Same as **a** for a model with a 2 km thick sedimentary layer and a Moho boundary at 48 km. **c** The model with the best fit contains a 5 km thick sedimentary layer and a Moho boundary at 49 km. Ps_sed: conversion from the bottom of a sedimentary layer, Ps_Moho: conversion from the Moho boundary; PpPs_Moho: the first Moho multiple with positive amplitude

Zagros crust along the MZT. A more recent study based on S receiver functions (Mohammadi. *et al.*, 2013) clearly imaged a significant crustal thickening (∼70 km) beneath the SSZ and resolved the presence of two different lithospheric blocks beneath Iran separated in the northeast of the UDMA (along a profile crossing northwest Zagros). Shad Manaman and Shomali (2010) showed similar results beneath the ZFTB (∼45 km) and SSZ using a partitioned waveform inversion method. Based on residual Bouguer anomalies, Jiménez-Munt *et al.* (2012) indicated a maximum crustal thickness of about

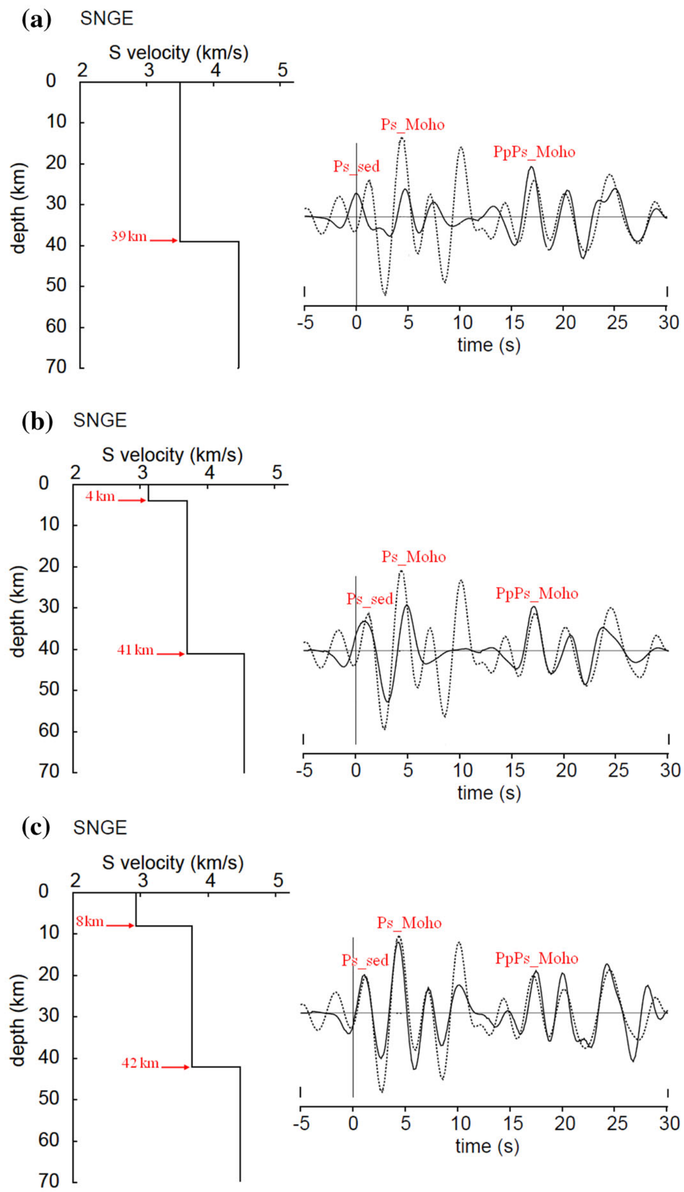

Figure 8
Same as Fig. 7 for station SNGE located in the SSZ

60 km beneath the Zagros collision zone between Fars and Lurestan arcs. Furthermore, they argued that the crust thins towards the Central Iran block and Persian Gulf and reaches about 42 km. We found an average crustal thickness of about 46 ± 2 km beneath UDMA, which is also supported by the results shown by Paul *et al*. (2006, 2010), Shad Manaman and Shomali (2010), Afsari *et al*. (2011), and Tatar and Nasrabadi (2013).

6.3. *Central Iran*

The Central Iranian Micro-Continent (CIMC) consists of separated blocks that drifted from Gondwana in the Permian to early-Triassic, and subsequently accreted onto Eurasia along the Alborz and Kopeh-Dagh sutures during the late Triassic closure of the Paleo-Tethys (Falcon 1974; Stoneley 1981). Based on our findings (Fig. 10c), the average

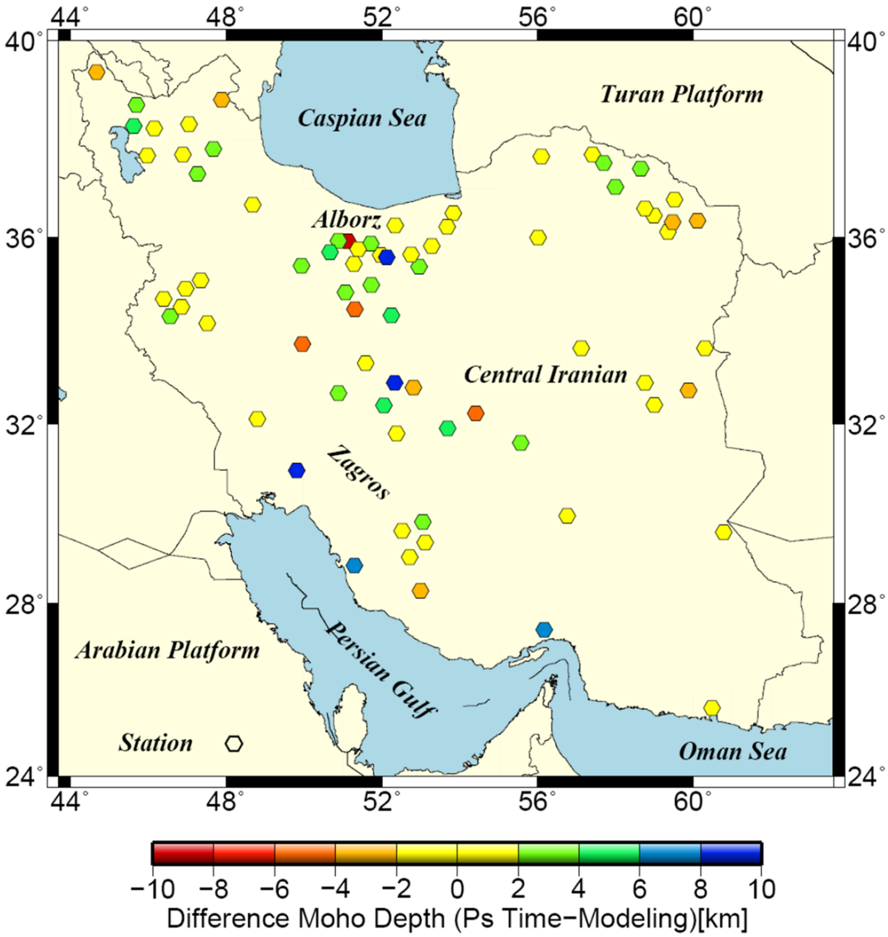

Figure 9
Differences between the estimated Moho depths calculated by Ps arrival time (according to velocity models presented in Table 2) and those obtained from Zhu and Kanamori approach (2000)

Moho depth beneath Central Iran, from the north to the south, varied between 42 ± 2 to 46 ± 2 km. However, our results were obtained only from few stations, but are in good agreement with the results indicated by Paul *et al*. (2006, 2010), Shad Manaman and Shomali (2010), Afsari *et al*. (2011), and Motavalli-Anbaran *et al*. (2011). Sodoudi *et al*. (2009) calculated the PRFs beneath the northern part of Central Iran. Using IASP91 reference model, they estimated the Moho at about 51 km depth, which is deeper than our estimate. The reason for this difference is related to the IASP91 model, which is relatively faster than the average velocity model we used for Central Iran (see Table 2). Beneath Azarbaijan (see Fig. 1), which is located in the northwestern part of Central Iran between two thrust belts—the Caucasus to the north, and the Zagros mountain belt to the south—we found an average crustal thickness of about 45 ± 2 km in good agreement with the results shown by Mangino and Priestley (1998). According to Fig. 10c, the Moho depth increases from west to east. It is not completely flat and increases smoothly from 40 ± 2 km under the Urumieh Lake in the west to about 50 ± 2 km in the east of the region. There is also a decrease in the Moho depth towards north. The Moho depth map presents a crustal thickening towards the northeast. Taghizadeh-Farahmand *et al*. (2010) attributed this variation to the collision between Central Iran and South Caspian plate, which most likely shows the crustal shortening processing in this part of Iran. Our estimations are also consistent with those obtained

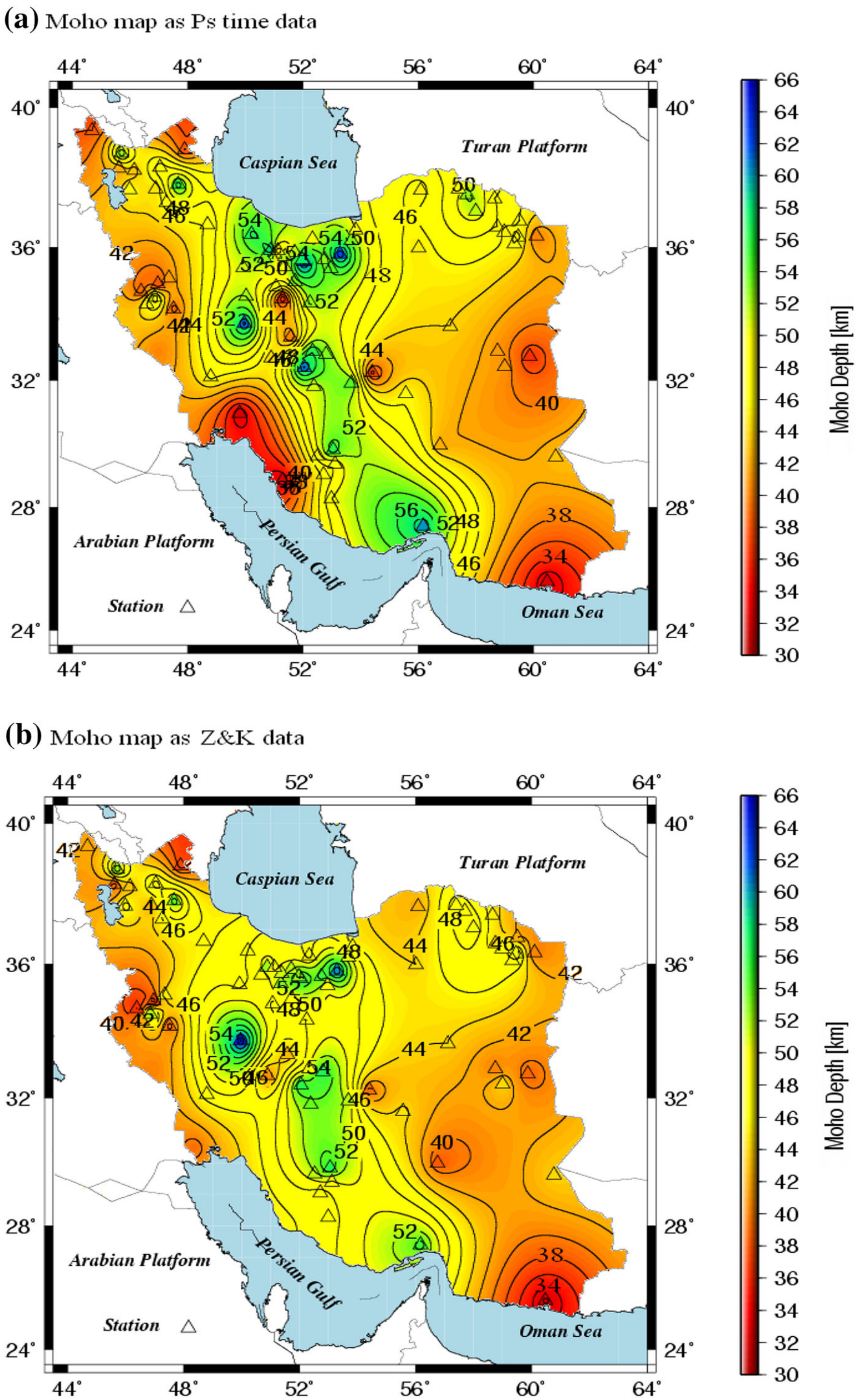

Figure 10
The Moho depth map (in km) obtained from P receiver function analysis. **a** using Ps arrival time, **b** using Z&K approach, and **c** using forward modeling

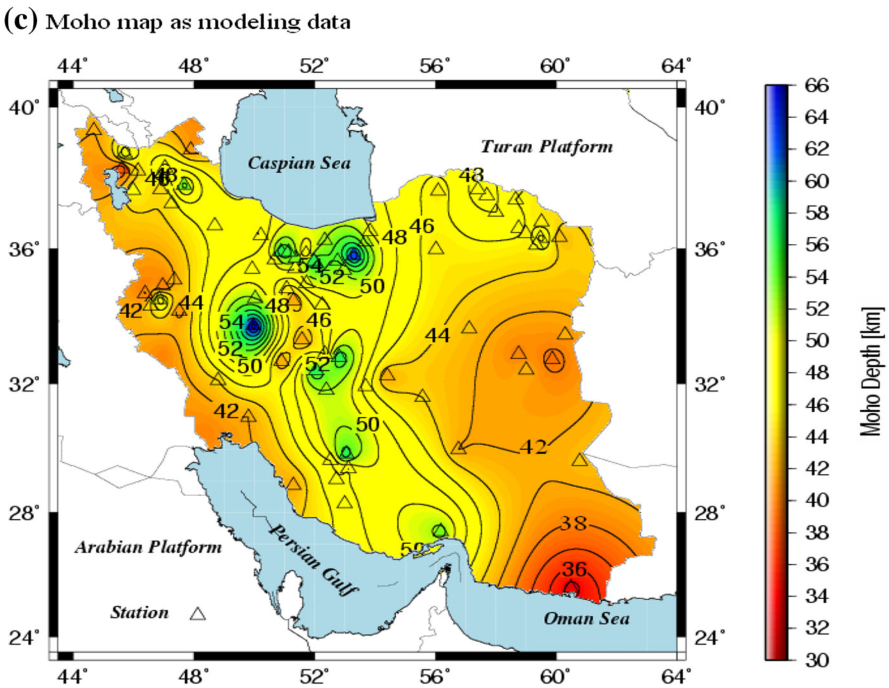

Figure 10
continued

from a joint inversion of PRFs and Rayleigh waves beneath NW Iran (NASRABADI *et al.*, 2011) and those shown beneath eastern Turkey (~45 km) (e.g. ZORE *et al.*, 2003; ANGUS *et al.*, 2006). Furthermore, our results beneath the eastern part of Central Iran (~42 ± 2 km) are consistent with those shown by NASRABADI *et al.* (2011), RAJAB-BEIKI *et al.* (2011) and JIMÉNEZ-MUNT *et al.* (2012).

6.4. Southeastern Iran (Makran)

The Makran region is the Oceanic-Continental subduction zone which is located in southeastern Iran and southern Pakistan. It is expanded ~1,000 km from west (Iran) to east (Pakistan) and its width is around 300 km. The north border reaches the Jazmoorian depression, and the southern range of this zone is limited to the Oman seacoast (Fig. 1). Few geophysical studies have focused on the Makran subduction zone, which mostly resolved the shallow seismic structure of this zone. Unfortunately, our estimation is bounded to the result of only one station (CHBR) showing the thinnest crust (~33 ± 2 km) within Iran. A crustal thickness of 33 km is very close to the average thickness of the continental crust and may show that the crust beneath this area has not been significantly thickened. This result is in good correlation with the absence of collisional processes beneath this region. DEHGANI and MAKRIS (1984) estimated the Bouguer anomaly for the whole Iranian plate and implied a crustal thickness of ~30 km beneath the Makran region. Moreover, our result is consistent with the results shown by SHAD MANAMAN *et al.* (2011), who found a thin crust (25–30 km) under the Oman seafloor and Makran foreacre setting. A PRF study beneath the western end of the Makran prism (YAMINI-FARD and HATZFELD, 2008) showed also the Moho boundary at ~32 km depth.

7. Conclusions

PRFs were calculated for the teleseismic events recorded between 1995-2011 at 77 national permanent stations (24 broadband and 53 short period) of Iran. We presented the first Moho depth map by forward modeling of PRFs. Our estimated Moho depth values coincided fairly well with those obtained from previous analysis using different geophysical approaches. Because of the different deformation zones existing in the study area, our results showed significant variations of the Moho depth beneath the Iranian plate. The maximum Moho depth ($\sim 66 \pm 2$ km) was seen along the Zagros mountain belt beneath the SSZ, where the crust of Central Iran is assumed to overthrust the Zagros crust along the MZT. The average crustal thickness beneath the ZFTB and the SSZ was estimated to be about 43 ± 2 km and 50 ± 2–55 ± 2 km, respectively. In general, we found average crustal thicknesses of about 40 ± 2 to 45 ± 2 km beneath the Iranian plate increasing northwards to about 50 ± 2 km beneath the Alborz Mountains, and up to 56 ± 2 km near the Damavand volcano due to the shortening process related to the orogenic belt. The crustal thickness ranges between 40 ± 2 and 44 ± 2 km beneath the Central Iran decreasing towards the SE and reaching about 33 ± 2 km beneath the Makran region, due to the lack of significant collisional processes. The Moho depth increases northwards to the Kopeh-Dagh Mountains with values varying between 43 ± 2 and 50 ± 2 km.

Acknowledgments

Authors are grateful to the Iranian Seismological Center (ISC) and the International Institute of Earthquake Engineering and Seismology (IIEES) for providing the teleseismic waveforms. We would like to thank Brian Mitchell and three anonymous reviewers for their constructive comments. We would also thank Ivone Jiménez-Munt for providing the fault map. We used the software packages Seismic Handler (Stammler, 1993) for data processing and GMT (Wessel and Smith 1998) for plotting, respectively. This research was supported by the Islamic Azad University, Qom branch.

References

Abbassi, A., Nasrabadi, A., Tatar, M., Yaminifard, F., Abbassi, M., Hatzfeld, D. and Priestley, K. (2010), Crustal velocity structure in the southern edge of the Central Alborz (Iran), J. Geodyn., *49,* 68–78.

Afsari, N., Sodoudi, F., Taghizadeh-Farahmand, F. and Ghassemi, M. R. (2011), Crustal structure of Northwest Zagros (Kermanshah) and Central Iran (Yazd and Isfahan) using teleseismic Ps converted phases, J. Seismology, *15*:341–353. doi:10.1007/s10950-011-9227-x.

Ammon, C. J. (1990), On the nonuniqueness of receiver function inversions, J. Geophys. Res., *95*, 2504–2510.

Angus, D. A., Wilson, D. C., Sandvol, E, Ni, J. F. (2006), Lithospheric structure of the Arabian and Eurasian collision zone in eastern Turkey from S-wave receiver functions. Geophys J. Int., *166*:1335–1346. doi:10.1111/j.1365-246X.2006.03070.x.

Asudeh, I. (1982), Seismic structure of Iran from surface and body wave data, Geophys. J. R. Astr., *71*, 715–730.

Azhari, S. M., Gheitanchi, M. R. and moeini, H. (2012), Crustal velocity model study beneath Shiraz seismic network using inversion of local earthquake travel times, 15th Iranian Geophysical Conference (IGC-15), Tehran University, Tehran, Iran.

Bassin, C., Laske, G. and Masters, G., 2000, The Current Limits of Resolution for Surface Wave Tomography in North America, EOS Trans AGU., 81, F897.

Beghoul, N., and Barazang M. (1989), Mapping High Pn Velocity Beneath the Colorado Plateau constrains uplift models, J. Geophys. Res., *94*, 7083–7104, 1989.

Berberian, M., (1995), Master blind thrust faults hidden under the Zagros folds: active basement tectonics and surface morphotectonics, Tectonophysics,*241,* 193–224.

Berberian, M., and Yeats, R.S., (1999), Patters of historical earthquake rupture in the Iranian plateau, Bul. Seism. Soc. Am., *89*, 120–139.

Bird, P. (1978), Finite element modeling of lithosphere deformation: the Zagros collision orogeny. Tectonophysics *50*, 307–336.

Boulin, J. (1991), Structures in southwest Asia and evolution of the eastern Tethys, Tectonophysics, *196*,211–268.

Dehgani, G. A. and Makris, J. (1984), The Gravity field and crustal structure of Iran, N. Jb. GeoL. Palaont Abh., *168*, 215–229.

Dewey. J. F., Hemton, M. R., Kidd, W. S. F., Saroglu, F. and Sengor A. M. C. (1986), Shortening of continental lithosphere: The neotectonicsof eastern Anatolia, a young collision zone, in Collision Tectonics, edited by M. P. Coward and A. C. Ries, Geol. Soc. Spe. Publ., *19*, 3–36.

Falcon, N.L. (1974), Southern Iran: Zagros mountains. Spec. Pub. Geol. Soc. Lond. *4*, 199–211.

Hatzfeld, D., Tatar, M., Priestley, K. and Ghafory-Ashtyany, M. (2003), Seismological constraints on the crustal structure beneath the Zagros mountain belt (Iran), Geophysical Journal International, *155*, 403–410.

Hessami, KH., Jamali, F., and Tabassi, H. (2003), Major Active Faults of Iran, International Institute of Earthquake Engineering and Seismology, Department of Seismotectonic, Seismology Research Center, Tehran, Iran.

Jackson, J. A., and McKenzi, D. P. (1984), Active tectonics of the Alpine-Himalayan belt between Western Turkey and Pakistan, Geophys. J. R. astr. Soc., *77*, 185–264.

Jackson, J., Priestley, K., Allen, M., and Berberian, M. (2002), Active tectonics of the South Caspian Basin, Geophys. J. Int., *148*(2), 214–245.

Javan Doloei, G. and Roberts, R. (2003), Crust and uppermost mantle structure of Tehran region from analysis of teleseismic P-waveform receiver functions, Tectonophysics, *364*, 115–133.

Jiménez-Munt, I., Fern'andez, M., Saura, E., Vergés, J., and Garcia-Castellanos, D. (2012), 3-D lithospheric structure and regional/residual Bouguer anomalies in the Arabia–Eurasia collision (Iran), Geophys. J. Int., *190*, 1311–1324. doi: 10.1111/j.1365-246X.2012.05580.x.

Kind, R., Kosarev, G. L., and Petersen, N. V., (1995), Receiver functions at the stations of the German Regional Seismic Network (GRSN), Geophys. J. I., *121*, 191–202.

Kumar, P., Yuan, X., Kumar, M.R., Kind, R., Li, X., and Chadha, R. K. (2007), The rapid drift of the Indian tectonic plate, Nature, *449*:894–897. doi:10.1038/nature06214.

Mangino, S., and Priestley, K. (1998), The crustal structure of the southern Caspian region, Geophys. J. Int., *133*:630–648.

Mohammadi, E., Sodoudi, F., Kind, R., Rezapour, M. (2013), Presence of a layered lithosphere beneath the Zagros collision zone, Tectonophysics, *608*, 366–375. doi:10.1016/j.tecto.2013.09.017.

Mohammadi, N., Sodoudi, F., Mohammadi, E., and Sadidkhouy, A. (2013), New constraints on lithospheric thickness of the Iranian Plateau using converted waves, J. Seismology, doi:10.1007/s10950-013-9359-2.

Mooney, W. D., Laske, G. and Masters, G., 1998, A Global crustal model at 5×5 degree, J. Geophys. Res., *103*, 727–747.

Motaghi, K., Tatar, M., and Priestley, K. (2012), Crustal thickness variation across the northeast Iran continental collision zone from teleseismic converted waves, J. Seismol., *16*:253–260, doi:10.1007/s10950-011-9267-2.

Motavalli-Anbaran, S. H., Zeyen, H., Brunet, M. F., and Ebrahimzadeh Ardestani, V. (2011), Crustal and lithospheric structure of the Alborz Mountains, Iran, and surrounding areas from integrated geophysical modeling, TECTONICS, VOL:*30*, doi:10.1029/2011TC002934.

Nasrabadi, A., Tatar, M. and Kaviani, A. (2011), Crustal Structure of Iran from Joint Inversion of Receiver Function and Phase Velocity Dispersion of Rayleigh Wave, Geosciences, No 82.

Paul, A., Kaviani, A., Hatzfeld, D., Vegne, J. and Mokhtari, M. (2006), Seismological evidence for crustal- scale thrusting in the Zagros mountain belt (Iran), Geophys J. Int., *166*:227–237. doi:10.1111/j.1365-24x.2006.02920.x.

Paul, A., Hatzfeld, D., Kaviani, A., Tatar, M., and Péquegnat, C. (2010), Seismic imaging of the lithospheric structure of the Zagros mountain belt (Iran), Geol. Soc. London Special Publications, *330*:5–18.

Radjaee, A.H., Rham, D., Mokhtari, M., Tatar, M., Priestley, K., and Hatzfeld, D. (2010), Variation of Moho depth in the Central part of Alborz Mountains, North of Iran, Geophys. J. Int., *181,* 173–184. doi:10.1111/j.1365-246X.2010.04518.x.

Rajab-Baiki, F., Afsari, N., Taghizadeh-Farahmand, f. and Gheitanche, M. R. (2011), Variations of the Moho depth and Vp/Vs ratio beneath East Iran (Birjand) using P receiver function method, Iranian Journal of Geophysics, Vol. 5, No. 1.

Richards, J. P., Wilkinson, D., and Ullrich, T. (2006) Geology of the Sari Gunay Epithermal Gold Deposit, Northwest Iran, Economic Geology, *101*(8), 1455–1496.

Shad Manaman, N., Shomali, H. (2010), Upper mantle S-velocity structure and Moho depth variations across Zagros belt, Arabian-Eurasian plate boundary. Phys Earth planet Inter., *180*, 92–103.

Shad Manaman, N., Shomali, H., and Hemin, K. (2011), New constraints on upper-mantle Svelocity structure and crustal thickness of the Iranian plateau using partitioned waveform inversion, Geophys J Int *184*: 247-267. doi:10.1111/j.1365-246X.2010.04822.x.

Snyder, D.B., and Barazangi, M. (1986), Deep crustal structure and flexture of the Arabian plate beneath the Zagros collisional mountain belt as inferred from gravity observation. Tectonics *5*:361–373.

Sodoudi, F., Yuan, X., Kind, R., Heit, B., and Sadidkhouy, A. (2009), Evidence for a missing crustal root and a thin lithosphere beneath the central Alborz by receiver function studies, Geophys. J. Int., *177*, 733–742. doi:10.1111/j.1365-246X.2009.04115.x.

Stammler, K. (1993), Seismichandler-programmable multichannel data handler for interactive and automatic processing of seismological analyses, Comput. Geosci., *19*:135–140.

Stoneley, R. (1981), The geology of the Kuh-e Dalnesh area of Southern Iran, and its bearing on the evolution of Southern Tethys. J Geol Soc Lond *138*:509–526.

Taghizadeh-Farahmand, F., Sodoudi, F., Afsari, N. and Ghassemi, M. R. (2010), Lithospheric structure of NW Iran from P and S receiver functions, J. Seismology, *14*:823–836. doi:10.1007/s10950-010-9199-2.

Taghizadeh-Farahmand, F., Sodoudi, F., Afsari, N., and Mohammadi, N. (2013), Receiver function images from the Moho and the LAB beneath the Kopeh-Dagh (Northeast Iran), J. Seismology, Vol *17*, No:3, doi:10.1007/s10950-013-9388-x.

Tatar, M. and Nasrabadi, A. (2013), Crustal thickness variations in the Zagros continental collision zone (Iran) from joint inversion of receiver functions and surface wave dispersion, J. Seismology, *17*. doi:10.1007/s10950-013-9394-z.

Vernant, Ph., Nilforoushan, F., Hatzfeld, D., Abbassi, M. R., Vigny, C., Masson, F., Nakali, H., Martinod, J., Ashtiani, A., Bayer, R., Tavakoli, F. and Chery J., (2004), Presentday crustal deformation and plate kinematics in the Middle East contrained by GPS measurements in Iran and northern Oman.Geophys. J. Int. *157*, 381–398.

Vernant, Ph. and Chéry, J., (2006), Mechanical modelling of oblique convergence in the Zagros, Iran, Geophys. J. Int., *165*, 991–1002.

Vinnik, L. P., (1977), Detection of waves converted from P to SV in mantle, Phys. Earth Planet. Inter., *15*, 39–45.

Wessel, P., and Smith, W. H. F. (1998), New, improved version of Generic Mapping Tools Released. EOS Trans Am Geophys Union *79*:579.

Yamini-Fard, F., and Hatzfeld, D. (2008), Seismic Structure Beneath Zagros-Makran Transition Zone (Iran) from Teleseismic Study: Seismological Evidence for Underthrusting and Buckling of the Arabian Plate Beneath Central Iran, JSEE, Vol. *10*, No. 1.

Yuan, X., Ni, J., Kind, R., Mechie, J., and Sandvol, E. (1997), Lithospheric and upper mantle structure of southern Tibet from a seismological passive source experiment. J Geophys Res *102* (27): 491–500.

Zamanian, H., Bayram-nejad, E., and Gheitanchi, M .R. (2012), Crustal Velocity Structure In Central of Iran Using Local

Earthquakes, 15th Iranian Geophysical Conference (IGC-15), Tehran University, Tehran, Iran.

ZHU, L. and KANAMORI, H. (2000), Moho depth variation in southern California from telesiesmic receiver, J. Geophys. Res., *105*, 2969–2980.

ZORE, E., SANDOVL, E., GURBUZ, C., TURKELLI, N., SEBER, D., and BARAZANGI, M. (2003), The crustal structure of the East Anatolian Plateau (Turkey) from receiver functions, J. Geophys. Res., *30*. doi:10.1029/2003GL018192.

(Received January 27, 2014, revised July 9, 2014, accepted July 10, 2014, Published online August 13, 2014)